Mon. Not. R. Astron. Soc. **360,** 465–476 (2005) doi:10.1111/j.1365-2966.2005.09002.x

Influence of the Coriolis force on the instability of slowly pulsating B stars

R. H. D. Townsend[1,2]★

[1]*Bartol Research Institute, University of Delaware, Newark, DE 19716, USA*
[2]*Department of Physics & Astronomy, University College London, Gower Street, London WC1E 6BT*

Accepted 2005 March 7. Received 2005 February 21; in original form 2004 November 11

ABSTRACT

This paper explores the effect of rotation on the κ-mechanism instability of slowly pulsating B stars. A new non-adiabatic code, which adopts the so-called traditional approximation to treat the Coriolis force, is used to investigate the influence exerted by rotation over the stability of stellar models covering the mass range $2.5\,\mathrm{M}_\odot \leqslant M_* \leqslant 13.0\,\mathrm{M}_\odot$. The principal finding is that, for all modes considered apart from the prograde sectoral (PS) class, rotation shifts the κ-mechanism instability toward higher luminosities and effective temperatures; these shifts are accompanied by broadenings in the extent of instability strips. Such behaviour is traced to the shortening of mode periods under the action of the Coriolis force. Instability strips associated with PS modes behave rather differently, being shifted to marginally lower luminosities and effective temperatures under the influence of rotation.

The implications of these results are discussed in the context of the observational scarcity of pulsation in B-type stars having significant rotation; various scenarios are explored to explain the apparent dichotomy between theory and observations. Furthermore, the possible significance of the findings to Be stars is briefly examined.

Key words: methods: numerical – stars: early-type – stars: emission-line, Be – stars: oscillations – stars: rotation – stars: variables: other.

1 INTRODUCTION

The slowly pulsating B (SPB) stars are a homogeneous class of mid-B-type, main-sequence objects that exhibit multiperiodic light and line-profile variations over time-scales on the order of 1–5 d. Waelkens (1991) was the first to classify these stars as a distinct group of early-type non-radial pulsators, by combining under the same aegis the photometric variables discovered by Waelkens & Rufener (1985) and the 53 Per spectroscopic variables first observed by Smith (1977). The theoretical pulsation characteristics of these objects have since been studied extensively, resulting in a canonical picture (see, e.g., Pamyatnykh 1999, and references therein) of high-order g-mode pulsation, driven by the same iron-group κ mechanism responsible for the instability of the β Cep pulsators (Dziembowski & Pamyatnykh 1993).

One outstanding issue in the understanding of SPB stars is the effect rotation has on their instability. Photometric surveys of open clusters by Balona (1994), Balona & Koen (1994) and Balona & Laney (1995, 1996) failed to find any evidence for SPB-like variability, but the authors did note that the stars observed were characterized by moderate or rapid projected equatorial rotation velocities ($v \sin i \gtrsim 100\,\mathrm{km\,s^{-1}}$). This result has led some to suggest that rotation suppresses the κ-mechanism excitation of g modes (see, e.g., Balona 2000). However, an alternative interpretation has been explored by Townsend (2003b), who examined the effect of the rotation-originated Coriolis force on the flux perturbations produced by low-frequency g modes. He demonstrated that the confinement of these modes within an equatorial waveguide (e.g. Lee & Saio 1990; Townsend 2003a) reduces the amplitude of the resulting photometric variations, possibly to below the sensitivity of the observations.

This paper addresses the SPB-rotation question from a more theoretical perspective, by examining the effect the Coriolis force has on the κ-mechanism instability of SPB stars. The high-order g modes excited in these objects are characterized by low frequencies and their dynamics can thus be expected to be influenced appreciably by the Coriolis force (see Townsend 2004). For this reason, canonical approaches that treat the rotation as a small perturbation to the pulsation (e.g. Carroll & Hansen 1982; Unno et al. 1989, their section 19 and references therein) are not well suited to SPB stars. Building on a methodology originated by Lee & Saio (1987a,b), alternative treatments have emerged over the past decade (see, e.g., Lee 1998, 2001); however, these are characterized by such a high degree of mathematical and numerical complexity, that their large-scale application is, with present-day computational resources, impractical.

The approach adopted herein aims at a compromise between sophistication and practicality, by employing an approximate method to treat the pulsation–rotation interaction (Section 2) that is well suited to the g modes found in SPB stars. This approach is applied to a range of B-type stellar models (Section 3), with the results of

★E-mail: rhdt@bartol.udel.edu

these stability calculations presented in Section 4. The findings of the analysis are then discussed and summarized in Section 5.

2 METHOD

2.1 Theoretical treatment

From a theoretical standpoint, the introduction of rotation significantly complicates the analysis of stellar pulsation. The centrifugal force tends to distort the equilibrium star away from a spherical configuration, and the Coriolis force leads to mixing between the radial and angular components of the fluid momentum. Both of these processes mean that the linearized equations describing non-radial, non-adiabatic pulsation are no longer separable in all coordinates, leading to a significant increase in the computational effort necessary for their solution (see, e.g., Lee 2001).

However, for the case of the low-frequency g modes found in SPB stars, an approximate treatment of the Coriolis force can be used to restore the separability of the pulsation equations and thereby render the problem tractable even with modest computing resources. At the heart of this approach is the so-called traditional approximation, introduced in a geophysical context by Eckart (1960) and first applied to stellar pulsation by Lee & Saio (1987a). The traditional approximation involves neglecting the polar component of the rotation angular frequency vector $\mathbf{\Omega}$, in the Coriolis terms of the linearized momentum equation. As discussed by Lee & Saio (1997), this approximation is reasonable throughout regions where the pulsation frequency σ (as measured in the corotating frame) and the rotation frequency Ω are both very much less than the Brunt–Väiäsäla frequency $\mathcal{N}$ associated with the gravitational stratification of the medium. In the case of g modes in B-type stars, this condition is fulfilled in almost all of the stably stratified, radiative envelope where the modes are propagative.

In addition to the traditional approximation, the treatment presented herein requires a number of other simplifications to permit the separation of the pulsation equations in all three spherical-polar coordinates $\{r, \theta, \phi\}$. These simplifications, which follow the analysis by Townsend (2003b), are as follows.

(i) The assumption that the rotation[1] is slow enough for both the centrifugal force and the departures from sphericity engendered by it to be neglected. In this context, slow may be interpreted as the condition $\Omega^2 \ll \Omega_c^2$, where

$$\Omega_c \equiv \sqrt{\frac{8GM_*}{27R_*^3}} \tag{1}$$

defines the critical rotation frequency within the Roche model, with M_* and R_* being the stellar mass and radius, and G the gravitational constant.

(ii) The Cowling (1941) approximation, whereby perturbations to the gravitational potential are neglected. This approximation is reasonable for all but low-order, low-degree modes.

(iii) The non-adiabatic radial flux (NARF) approximation, whereby the divergence of the horizontal Eulerian flux perturbation is neglected in the energy equation. As demonstrated by Townsend (2003b), this approximation, first introduced by Savonije, Papaloizou & Alberts (1995), is valid under the same conditions ($\sigma, \Omega \ll \mathcal{N}$) as the traditional approximation itself.

[1] Assumed throughout to be uniform.

(iv) The steady-wave approximation, whereby the imaginary part σ_i of the pulsation frequency σ is neglected in solving the angular parts of the pulsation equations. This approximation, which is discussed by Townsend (2000), is appropriate when the growth rate of the pulsation is slow, so that σ_i is very much smaller than the corresponding real part σ_r of the pulsation frequency.

This collection of approximations and assumptions closely follows those employed by Ushomirsky & Bildsten (1998), with the exception that their use of the quasi-adiabatic approximation is replaced herein by the adoption of the NARF approximation. This replacement is particularly significant, in that the quasi-adiabatic approximation can lead to incorrect results when applied to B-type stars (see, e.g., Dziembowski, Moskalik & Pamyatnykh 1993); in contrast, the NARF approximation is able to capture the essential physics of the non-adiabatic processes responsible for the κ-mechanism instability.

2.2 Pulsation equations

Within the approximations outlined in the preceding section, the spatial and temporal dependence of perturbed variables is expressed in the corotating frame as

$$f'(r,\ \mu,\ \phi,\ t) = f'(r)\,\Theta_\ell^m(\mu)\,\mathrm{e}^{\mathrm{i}(m\phi+\sigma t)} \tag{2}$$

and

$$\delta f(r,\ \mu,\ \phi,\ t) = \delta f(r)\,\Theta_\ell^m(\mu)\,\mathrm{e}^{\mathrm{i}(m\phi+\sigma t)}, \tag{3}$$

where: Eulerian and Lagrangian perturbations are represented by primes ($'$) and δ, respectively; t is the temporal coordinate; and $\mu \equiv \cos\theta$. Here, the Hough function $\Theta_\ell^m(\mu)$ is a solution to Laplace's tidal equation (see, e.g., Bildsten, Ushomirsky & Cutler 1996), which depends implicitly on the spin parameter $\nu \equiv 2\Omega/\sigma_r$ characterizing the relative strength of Coriolis and buoyancy forces (Townsend 2004). In the limit of no rotation, $\Theta_\ell^m(\mu)$ approaches the normalized Legendre function $\bar{P}_\ell^m(\mu)$ (see Lee & Saio 1990) having harmonic degree ℓ and azimuthal order m.

Inspired by the dimensionless formulations introduced by Saio & Cox (1980) and Lee & Saio (1997), which themselves are built on the seminal Dziembowski (1971) treatment, the radial dependencies $f'(r)$ and $\delta f(r)$ of perturbed variables are expressed in terms of a set of eigenfunctions $q_i (i = 1, 2, 5, 6)$,[2] such that

$$\frac{\xi_r(r)}{r} = q_1\,x^{\tilde{\ell}-2}, \quad \frac{p'(r)}{\rho g r} = q_2\,x^{\tilde{\ell}-2}, \tag{4}$$

$$\frac{\delta S(r)}{c_p} = q_5\,x^{\tilde{\ell}}, \quad \frac{\delta L_R(r)}{L_*} = q_6\,x^{\tilde{\ell}+1}. \tag{5}$$

Here, $x \equiv r/R_*$ is the dimensionless radial coordinate, ξ_r the radial fluid displacement, p' the Eulerian pressure perturbation, δS the Lagrangian perturbation to the specific entropy and δL_R the Lagrangian perturbation to the radial part of the radiative luminosity. Other symbols appearing in these expressions are defined by Unno et al. (1989), with the exception of the effective harmonic degree

$$\tilde{\ell} = \frac{\sqrt{1+4\lambda_\ell^m}-1}{2}, \tag{6}$$

[2] The indices 3 and 4 are traditionally reserved for the perturbation to the gravitational potential and its radial derivative; as a result of the adoption of the Cowling (1941) approximation, they are not used in the present analysis.

introduced by Townsend (2000) as the solution of the equation $\tilde{\ell}(\tilde{\ell}+1) = \lambda_\ell^m$. In these relations, λ_ℓ^m is the eigenvalue of Laplace's tidal equation associated with the Hough eigenfunction $\Theta_\ell^m(\mu)$. This eigenvalue depends implicitly on the spin parameter ν, and therefore on both the pulsation frequency σ and the rotation frequency Ω.

The radial eigenfunctions q_i are found as the solutions of four coupled, first-order differential equations:

$$x\frac{\mathrm{d}q_1}{\mathrm{d}x} = \left(\frac{V}{\Gamma_1} - 1 - \tilde{\ell}\right)q_1 + \left[\frac{\tilde{\ell}(\tilde{\ell}+1)}{c_1\omega^2} - \frac{V}{\Gamma_1}\right]q_2 + \upsilon_T x^2 q_5, \quad (7)$$

$$x\frac{\mathrm{d}q_2}{\mathrm{d}x} = \left(c_1\omega^2 - A^*\right)q_1 + \left(A^* - U + 3 - \tilde{\ell}\right)q_2 + \upsilon_T x^2 q_5, \quad (8)$$

$$\begin{aligned} x\frac{\mathrm{d}q_5}{\mathrm{d}x} &= V\left[\nabla_{\mathrm{ad}}\left(U - c_1\omega^2\right) - 4(\nabla_{\mathrm{ad}} - \nabla) + c_2\right]\frac{q_1}{x^2} \\ &\quad + V\left[\frac{\tilde{\ell}(\tilde{\ell}+1)}{c_1\omega^2}(\nabla_{\mathrm{ad}} - \nabla) - c_2\right]\frac{q_2}{x^2} \\ &\quad + \left[V\nabla(4 - \kappa_S) - \tilde{\ell}\right]q_5 - \frac{V\nabla}{l_{\mathrm{R}}}xq_6, \end{aligned} \quad (9)$$

$$\begin{aligned} x\frac{\mathrm{d}q_6}{\mathrm{d}x} &= -\varepsilon_{\mathrm{ad}}\bar{c}_3 V\frac{q_1}{x^3} + \left[\varepsilon_{\mathrm{ad}}\bar{c}_3 V + \frac{\tilde{\ell}(\tilde{\ell}+1)}{c_1\omega^2}x\frac{\mathrm{d}l_{\mathrm{R}}}{\mathrm{d}x}\right]\frac{q_2}{x^3} \\ &\quad + (\bar{c}_3\varepsilon_{\mathrm{S}} - \mathrm{i}\omega\bar{c}_4)\frac{q_5}{x} - \left(\tilde{\ell}+1\right)q_6. \end{aligned} \quad (10)$$

Here, the dimensionless pulsation frequency ω has the usual definition

$$\omega \equiv \sigma\sqrt{\frac{R_*^3}{GM_*}} \quad (11)$$

and all other symbols follow the nomenclature of Unno et al. (1989), with the exception of the introductions

$$l_{\mathrm{R}} \equiv \frac{L_{\mathrm{R}}}{L_*}, \quad (12)$$

$$\bar{c}_3 \equiv c_3\, l_{\mathrm{R}} = \frac{4\pi r^3\rho\varepsilon_{\mathrm{N}}}{L_*} \quad (13)$$

and

$$\bar{c}_4 \equiv c_4\, l_{\mathrm{R}} = \frac{4\pi r^3\rho T c_p}{L_*}\sqrt{\frac{GM_*}{R_*^3}}. \quad (14)$$

In the limit $\nu \to 0$, the effective harmonic degree $\tilde{\ell}$ approaches the true harmonic degree ℓ and the governing equations (7)–(10) reduce to those describing non-radial, non-adiabatic pulsation of a non-rotating star, within the NARF and Cowling (1941) approximations. However, even allowing for the alternative nomenclature, the energy conservation equation (10) in this limit appears rather different than in other non-adiabatic treatments (compare with, e.g., Unno et al. 1989, their equation 24.12[3]). In particular, the derivative of the dimensionless radiative luminosity l_{R} appears in the present treatment as a result of the choice of frozen convection approximation; this choice centres around neglecting perturbations to the convective source term in the linearized energy equation, as per equation (21.7) of Unno et al. (1989). Although Pesnell (1990) has argued that such an approach is unphysical, it is required to ensure the pulsation equations remain self-consistent at the origin. In any case, because g modes do not penetrate far into convective regions, any errors introduced by this convection-freezing choice should be minimal.

Solutions of the pulsation equations (7)–(10) are required to satisfy boundary conditions at the centre and at the surface. The inner conditions

$$\left.\begin{aligned} c_1\omega^2 q_1 - \tilde{\ell}\, q_2 &= 0 \\ 3l_{\mathrm{R}}\, q_1 - x^3 q_6 &= 0 \end{aligned}\right\} \quad \text{as } x \to 0 \quad (15)$$

ensure that solutions remain finite and regular at the origin. Likewise, the outer boundary conditions

$$\left.\begin{aligned} q_1 - q_2 &= 0 \\ (2 - 4\nabla_{\mathrm{ad}}V)\, q_1 + 4\nabla_{\mathrm{ad}}V\, q_2 + 4\, q_5 - q_6 &= 0 \end{aligned}\right\} \text{at } x = 1 \quad (16)$$

follow from the assumptions that the surface pressure tends to zero and that there is no flux incident from outside the star (see, e.g. Unno et al. 1989). Finally, the arbitrary overall scaling of solutions is constrained by the normalization condition

$$q_1 = 1 \quad \text{at } x = 1. \quad (17)$$

2.3 Implementation

To solve the pulsation equations (7)–(10) and accompanying boundary conditions (15)–(17), a wholly new Fortran 95 code was developed. The code, named BOOJUM, follows the root-finding approach pioneered by Castor (1971) and Osaki & Hansen (1973): one of the boundary conditions is set aside, allowing solution of the equations to be achieved at arbitrary dimensionless frequency ω. The suppressed boundary condition is then used to construct a discriminant $D(\omega)$, whose roots correspond to the eigenfrequencies of the full system of equations.

In the present case, the outer mechanical boundary condition is used to form the discriminant

$$D(\omega) = \frac{(q_1 - q_2)_{x=1}}{(q_1 + q_2)_{x=0}}. \quad (18)$$

The numerator is the boundary condition itself, while the denominator, which is guaranteed by the inner boundary conditions (15) never to be zero, ensures that the discriminant remains well behaved (see Townsend 2000). To calculate the solution vector q_i required to evaluate this discriminant, BOOJUM uses a standard relaxation approach (e.g. Press et al. 1992); because the pulsation equations are linear in q_i, only a single iteration is required at each value of ω. The $\tilde{\ell}$-dependent scalings, adopted in the definitions (4) of the eigenfunctions, successfully prevent the loss of precision near the centre discussed by Takata & Löffler (2004). For improved accuracy, centred finite differences are used in the relaxation algorithm; however, in regions where $\bar{c}_4 > 10^4$, BOOJUM switches to one-sided differences for the thermal equations (9)–(10), in accordance with the Sugimoto (1970) prescription for avoiding numerical stability (and see also Unno et al. 1989, their section 24).

Solution of the characteristic equation

$$D(\omega) = 0, \quad (19)$$

defining the eigenfrequencies of the pulsation equations, is accomplished in BOOJUM using the robust Traub (1964) implementation of the root-finding algorithm devised by Muller (1956); this algorithm is a generalization of the complex secant approach favoured by Castor (1971). Note that the latter author used approximate roots of the characteristic equation to find starting points for the solution,

[3] Note that the sign of the $c_3/c_1\omega^2$ term in their equation is incorrect.

via iterative relaxation, of the full pulsation equations. A somewhat simpler approach is adopted by BOOJUM, whereby equation (19) is solved to the desired fractional tolerance in ω (in the present work, 10^{-10} for both real and imaginary parts) and no additional calculations are performed.

For calculation of the λ_ℓ^m eigenvalue, required (cf. equation 6) to evaluate the $\tilde{\ell}$ terms appearing in the pulsation equations and boundary conditions, BOOJUM uses the matrix-mechanical approach pioneered by Lee & Saio (1987a). The implementation largely follows the procedure described by Townsend (2003b); however, the truncation dimension N is determined dynamically, by repeatedly doubling N until the fractional change in λ_ℓ^m drops below some specified threshold (taken to be 10^{-5} throughout the present work). Furthermore, the algorithm due to Kahan (1966), as implemented by the LAPACK subroutine library (Anderson et al. 1999), is used for calculating the matrix eigenvalues; this algorithm performs significantly better at finding isolated eigenvalues than the previously adopted *QL* approach.

As input, BOOJUM is supplied with the desired mode parameters (ℓ, m), the rotation angular frequency Ω and an indication of the region over which to search for eigenfrequencies satisfying the characteristic equation (19). The coefficients appearing in the pulsation equations and boundary conditions are evaluated using a precomputed stellar model (see Section 3); the model, typically composed of ca. 1000 radial points, is interpolated onto a new grid having 10 000 points, distributed non-uniformly via an approach similar to that described by Christensen-Dalsgaard & Mullan (1994, their appendix A3). Cubic splines are used for interpolating all variables apart from the Brunt–Väiäsäla frequency $\mathcal{N}$; the latter is interpolated linearly, to avoid the introduction of spurious oscillations in the molecular weight gradient zone situated outside the convective core.

3 STELLAR MODELS

The Warsaw—New Jersey stellar evolution code is used to calculate 115 tracks of stellar models, sampling the initial mass range $M_* = 2.5$–$5.2\,\mathrm{M}_\odot$ at a resolution $0.05\,\mathrm{M}_\odot$, the range $M_* = 5.2$–$9.2\,\mathrm{M}_\odot$ at a resolution $0.1\,\mathrm{M}_\odot$ and the range $M_* = 9.2$–$13.0\,\mathrm{M}_\odot$ at a resolution $0.2\,\mathrm{M}_\odot$; each track extends from zero-age main sequence (ZAMS) to terminal-age main sequence (TAMS). Details of the code have already been given by Dziembowski & Pamyatnykh (1993) and Dziembowski et al. (1993); the only significant difference in the present work is the adoption of more-recent OPAL tabulations for opacity (Iglesias & Rogers 1996) and the equation of state (Rogers, Swenson & Iglesias 1996). In all cases, the initial hydrogen and metal mass fractions are set at the canonical values $X = 0.7$ and $Z = 0.02$, with a heavy-element mixture taken from Grevesse & Noels (1993). No account is taken of the effect of rotation on the stellar evolution; although Pamyatnykh (1999) has demonstrated that rotation-induced mixing can shift the red edge of the SPB instability strip to lower effective temperatures, the present analysis is more concerned with the *dynamical* influence of rotation on SPB pulsation.

Each of the calculated evolutionary tracks is composed of approximately 42 stellar models, with a grand total of 4876 models for the entire set. Fig. 1 plots the positions of these models in the theoretical Hertzsprung–Russell (HR) diagram, along with the loci defining the ZAMS and TAMS boundaries. The dense model coverage of the main-sequence band is to facilitate the accurate positioning of instability strips (Section 4.2) in the $T_{\rm eff}$–L_* plane.

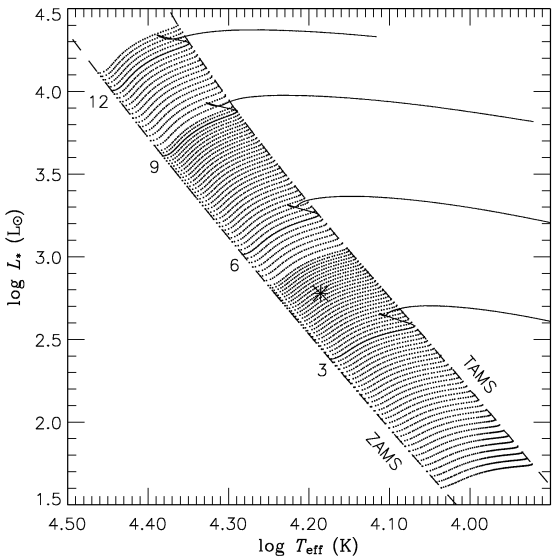

Figure 1. The theoretical Hertzsprung–Russell (HR) diagram for the stellar models introduced in Section 3; these are plotted as points in the effective temperature ($T_{\rm eff}$) versus stellar luminosity (L_*) plane. The dashed lines running diagonally from top left to bottom right indicate the zero-age main sequence (ZAMS) and terminal-age main sequence (TAMS) limits, while the asterisk shows the location of the 53 Per-like model analysed in Section 4.1. Full evolutionary tracks for four selected models are also shown in the diagram, plotted as solid lines and labelled by their corresponding stellar masses, in solar units. The two higher-mass tracks do not reach the low-temperature boundary of the diagram, because the Warsaw–New Jersey evolutionary code is unable to follow these models beyond the ignition of core helium burning.

Table 1. Fundamental parameters of the 53 Per-like stellar model analysed in Section 4.1.

$T_{\rm eff}$/K	$\log g$/cm s^{-2}	$L_*/\mathrm{L}_\odot$	$M_*/\mathrm{M}_\odot$	$R_*/\mathrm{R}_\odot$
15 300	4.04	600	4.80	3.48

4 STABILITY CALCULATIONS

4.1 53 Per model

From the models introduced in the preceding section, one is selected as having parameters close to the values inferred by De Ridder et al. (1999) for 53 Per, the archetypal SPB star; these parameters are documented in Table 1 and the corresponding position in the HR diagram is shown in Fig. 1 by an asterisk. This 53 Per-like model is employed to examine the general influence the Coriolis force exerts over $\ell = 1$ and $\ell = 2$ non-radial g modes. Eigenfrequencies of these modes are calculated using BOOJUM, for all possible values $-\ell \leqslant m \leqslant \ell$ of the azimuthal order and over a range of angular frequencies from the non-rotating case up to the intermediate rate $\Omega/\Omega_{\rm c} = 0.5$. This upper limit corresponds to a rotation period $\Pi = 1.26\,\mathrm{d}$, with an equatorial velocity $v_{\rm e}$ that is 35 per cent of the critical velocity $v_{\rm c} = 419\,\mathrm{km\,s^{-1}}$ of the star; by way of comparison, the most rapidly rotating SPB star known to date, HD 1976, rotates at ~32 per cent of its critical velocity (Mathias et al. 2001).

The results from these calculations are shown in Fig. 2, where the corotating frame period $P \equiv 2\pi/\sigma_{\rm r}$ of each mode is plotted as a function of rotation angular frequency. Points associated with

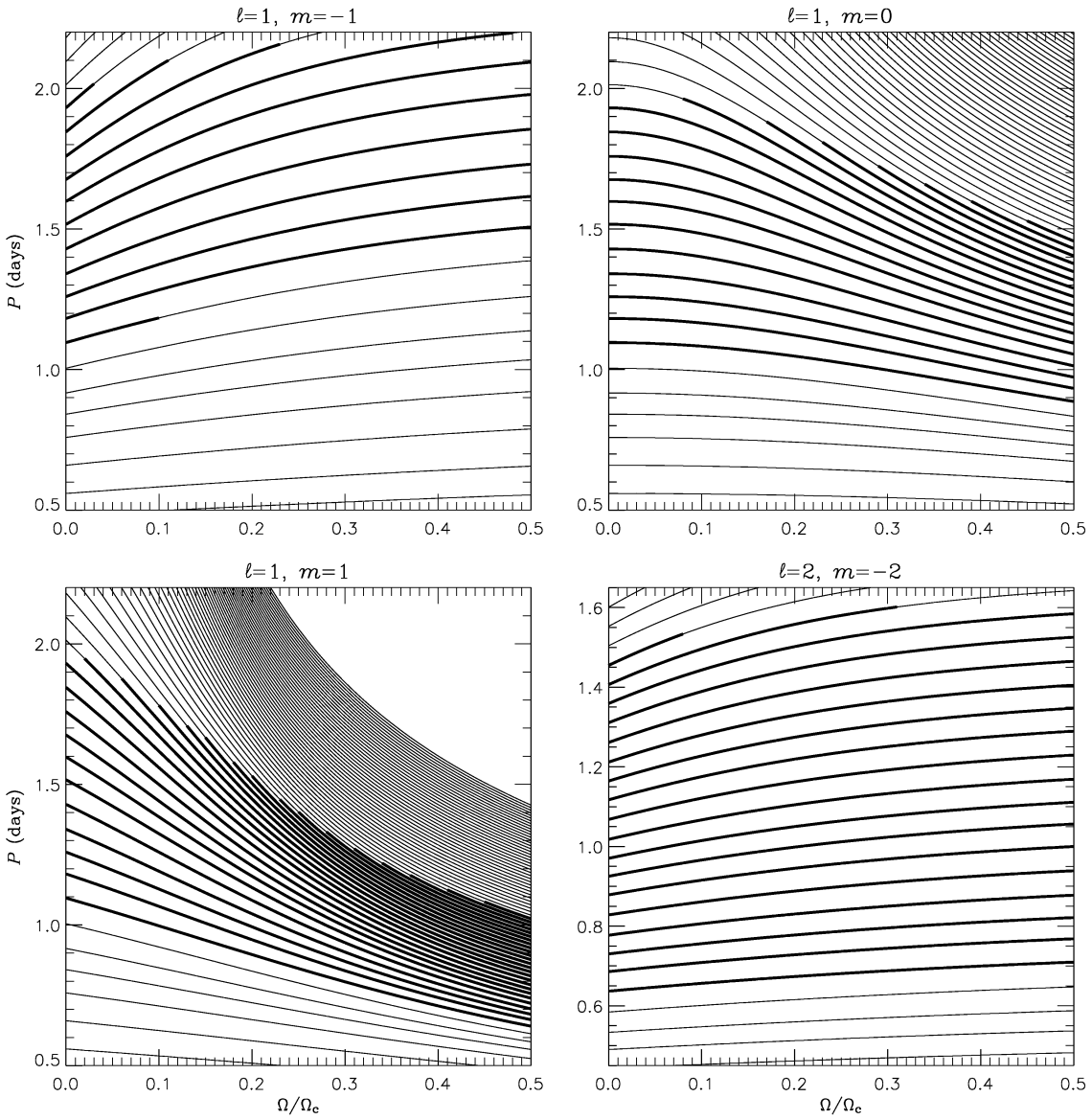

Figure 2. Pulsation periods for $\ell = 1$ and $\ell = 2$ g modes of the 53 Per-like model, plotted as a function of rotation frequency up to a maximum $\Omega = 0.5\,\Omega_c$. Each curve corresponds to a particular radial order $\tilde{n}$; the line weight is used to indicate whether modes are stable (thin) or unstable (thick) against the κ-mechanism instability. To improve the clarity of the figure, only radial orders $|\tilde{n}| \leqslant 75$ are plotted.

eigenfunctions q_i having the same radial order $\tilde{n}$[4] are linked together into a single, continuous curve; the weight of the curves, at each value of Ω, is used to indicate whether a mode is stable ($\sigma_i > 0$) or unstable ($\sigma_i < 0$) against κ-mechanism excitation.

At $\Omega = 0$, the eigenfrequencies are degenerate in azimuthal order m, owing to the arbitrariness of the polar axis of the model. This degeneracy is lifted upon the introduction of rotation, with a splitting initially following the first-order relation

$$\Delta\sigma_r \approx m\Omega C_{\tilde{n},\ell}, \tag{20}$$

or alternatively

$$\Delta P \approx -m\Pi C_{\tilde{n},\ell}, \tag{21}$$

derived by Ledoux (1951); here, $\Pi \equiv 2\pi/\Omega$ is the rotation period and Δ denotes the change in the indicated quantity. In the case of the high-order g modes considered herein, the term $C_{\tilde{n},\ell}$ approximates to $1/\ell(\ell+1)$, explaining why the $\ell = 1$ modes exhibit steeper gradients $\Delta P/\Delta\Omega$ around $\Omega \approx 0$.

Toward larger values of Ω, departures from the above linear relations are increasingly apparent in Fig. 2. For all apart from the prograde sectoral (PS) modes having $\ell = -m$, these departures produce an overall trend of decreasing pulsation period with increasing rotation rate, irrespective of whether the mode is prograde ($m < 0$), retrograde ($m > 0$) or zonal ($m = 0$). Such behaviour comes from the influence of the Coriolis force and can readily be understood by

[4] As defined by Unno et al. (1989, their equation 17.5), within the generalization to the Cowling (1941) nomenclature introduced by Scuflaire (1974) and Osaki (1975).

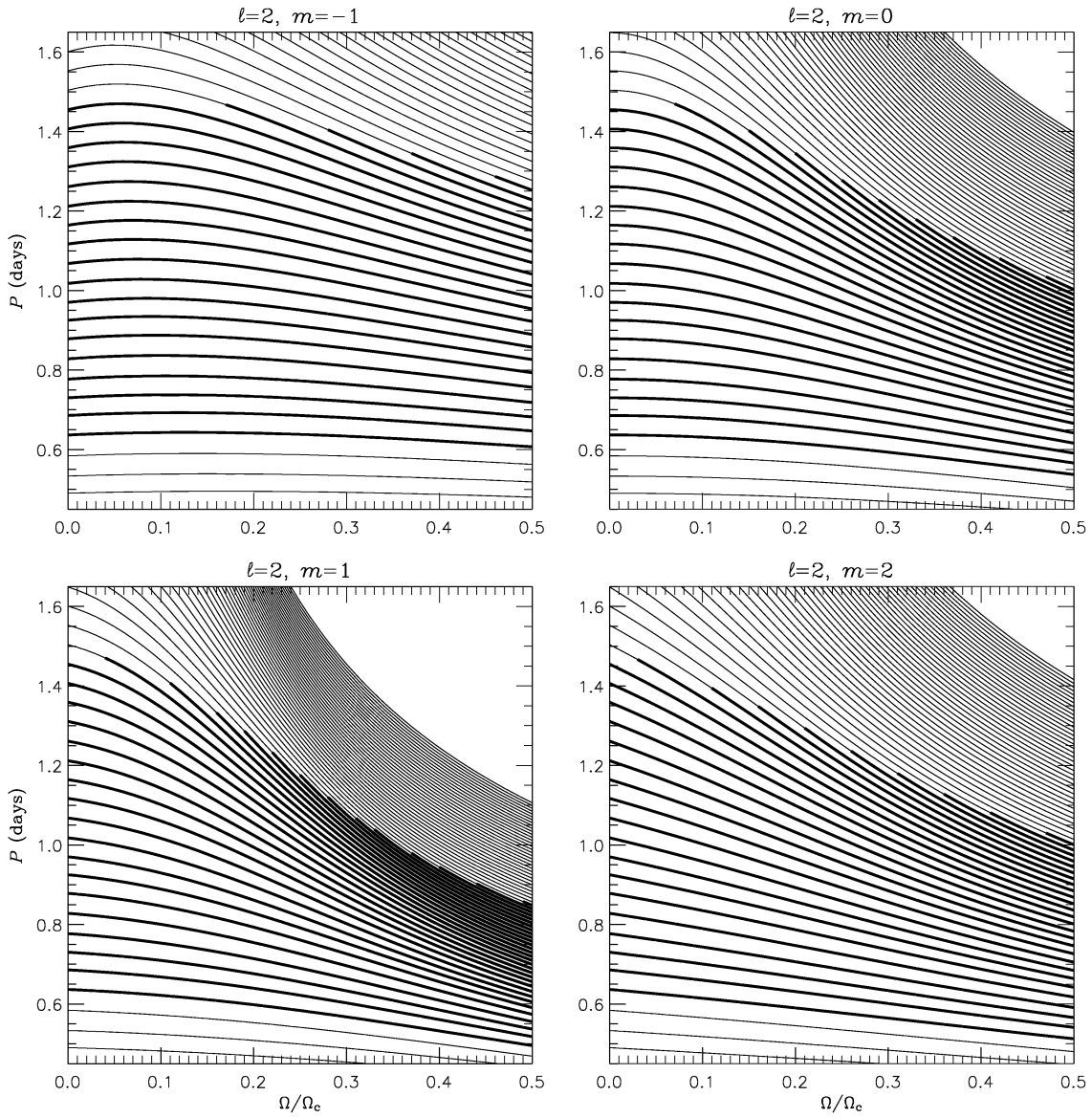

Figure 2 – *continued*

recalling that, at the most general level, the frequency of a wave may be expressed as the square root of the ratio between a generalized stiffness and a generalized inertia (see, e.g., Lighthill 1978). With the introduction of rotation, the stiffness[5] usually resulting from buoyancy is augmented by the Coriolis force; this leads to an increase in frequency and thence a corresponding *decrease* in mode period.

Because the strength of the Coriolis force varies with spin parameter ν, the effects described are differential: the periods of long-period, larger-ν modes are shortened by a far greater degree than those of short-period, smaller-ν modes. Accordingly, the density of the pulsation spectrum, as measured by the number of modes either per period interval or per frequency interval, increases markedly with rotation rate. As can be seen in Fig. 2, this spectral compression is especially pronounced for the $m = 1$ modes.

[5] That is, the restoring force on displaced fluid elements.

This latter result warrants some explanation. For non-PS modes in the inertial regime $|\nu| > 1$, the Coriolis force acts to confine the modes within an equatorial waveguide, whose boundaries are situated at $\mu = \pm 1/|\nu|$ (see, e.g., Bildsten et al. 1996). A requirement of the trapping is that the $s + 1$ nodes of the Hough function Θ_ℓ^m be fitted within these waveguide boundaries, where

$$s = \ell - |m| \pm 1 \tag{22}$$

is the meridional order introduced by Townsend (2003a). In this expression, the difference between the prograde and zonal modes ($m \leqslant 0$; minus sign) and the retrograde modes ($m > 0$; plus sign) comes about because an extra pair of nodes appears in the latter when $|\nu| > 1$ (see Lee & Saio 1990). In the limit $|\nu| \gg 1$, the fitting requirement is embodied in the angular characteristic equation

$$\lambda_\ell^m \approx \nu^2 (2s + 1)^2 \tag{23}$$

Table 2. Instability ranges for g modes of the 53 Per-like model; for each (ℓ, m) pair considered and at three differing rotation rates, the range of $|\tilde{n}|$ spanned by unstable modes is tabulated, along with the corresponding values of the corotating frame period P, the inertial frame period $P_{\rm i}$ (negative values in parentheses) and the harmonic degree ratio $\tilde{\ell}/\ell$. The absolute value of $\tilde{n}$ is used, because this radial order is negative for g modes.

(ℓ, m)	$\lvert\tilde{n}\rvert$	P (days)	$P_{\rm i}$ (days)	$\tilde{\ell}/\ell$
		$\Omega/\Omega_{\rm c} = 0.00$		
$(1,-1)$	12–22	1.10–1.93	1.10–1.93	1.00–1.00
$(1,0)$	12–22	1.10–1.93	1.10–1.93	1.00–1.00
$(1,1)$	12–22	1.10–1.93	1.10–1.93	1.00–1.00
$(2,-2)$	12–29	0.64–1.46	0.64–1.46	2.00–2.00
$(2,-1)$	12–29	0.64–1.46	0.64–1.46	2.00–2.00
$(2,0)$	12–29	0.64–1.46	0.64–1.46	2.00–2.00
$(2,1)$	12–29	0.64–1.46	0.64–1.46	2.00–2.00
$(2,2)$	12–29	0.64–1.46	0.64–1.46	2.00–2.00
		$\Omega/\Omega_{\rm c} = 0.25$		
$(1,-1)$	13–19	1.40–2.07	0.90–1.14	0.79–0.75
$(1,0)$	12–25	1.03–1.77	1.03–1.77	1.09–1.32
$(1,1)$	12–31	0.85–1.40	1.27–3.16	1.40–2.26
$(2,-2)$	12–28	0.68–1.58	0.44–0.70	1.84–1.74
$(2,-1)$	12–30	0.64–1.40	0.51–0.90	1.99–2.18
$(2,0)$	12–33	0.61–1.28	0.61–1.28	2.13–2.70
$(2,1)$	12–35	0.58–1.18	0.76–2.21	2.22–3.18
$(2,2)$	12–33	0.58–1.23	1.07–46.50	2.25–2.83
		$\Omega/\Omega_{\rm c} = 0.50$		
$(1,-1)$	13–18	1.51–2.10	0.69–0.79	0.72–0.69
$(1,0)$	12–29	0.89–1.46	0.89–1.46	1.32–2.00
$(1,1)$	12–38	0.64–1.04	1.30–5.76	1.99–4.02
$(2,-2)$	12–27	0.71–1.59	0.33–0.45	1.75–1.66
$(2,-1)$	12–33	0.61–1.25	0.41–0.63	2.12–2.77
$(2,0)$	12–38	0.54–1.00	0.54–1.00	2.46–4.17
$(2,1)$	12–42	0.50–0.85	0.82–2.59	2.71–5.58
$(2,2)$	12–38	0.51–1.00	2.73–(1.71)	2.60–4.18

for the Hough-function eigenvalue (Townsend 2003a, his equation 38), corresponding to an effective harmonic degree

$$\tilde{\ell} \approx \sqrt{\lambda_\ell^m} \approx \begin{cases} (2\ell - 2|m| - 1)\,\nu & (m \leqslant 0), \\ (2\ell - 2|m| + 3)\,\nu & (m > 0). \end{cases} \tag{24}$$

Regarding the ratio $\tilde{\ell}/\ell$ as a measure of the severity of equatorial confinement, this latter expression indicates $m = 1$ modes, for each value of ℓ, are the most affected by the Coriolis force. This result can be seen in the right-most column of Table 2 introduced below; physically, it follows directly from the fact that these modes have the largest meridional orders ($s = 1$ for $\ell = 1$ and $s = 2$ for $\ell = 2$) and are therefore the most compressed in the polar direction when squeezed into the equatorial waveguide.

The foregoing analysis does not apply to the PS modes, $(\ell, m) = (1, -1)$ and $(\ell, m) = (2, -2)$, whose periods lengthen somewhat toward larger Ω. As discussed by Townsend (2003a), this class of mode is transformed by the Coriolis force into equatorial Kelvin waves. Such waves have different properties than the usual gravito-inertial waves found in a rotating, stratified system; in particular, they are characterized by geostrophic balance, whereby the Coriolis force arising from azimuthal fluid motions is countered by polar pressure gradients (see, e.g., Gill 1982). As a result of this balance, the Coriolis force makes relatively little difference to the generalized stiffness of PS modes and therefore does not produce the marked period decrease seen for the other modes.

As a prelude to the analysis presented in the following section, the focus now turns briefly toward the *stability* of the modes plotted in Fig. 2. Once again, there is a dichotomy between the PS modes and the others: the former are partly stabilized by rotation and the latter partly destabilized. However, in both cases the rotation does not alter the property that a contiguous sequence of modes is unstable toward the κ mechanism. With this result in mind, Table 2 succinctly summarizes the data shown in the figure, by indicating the range of the instability, at three differing rotation rates, for each (ℓ, m) pair considered. This range is expressed in terms of the radial orders of the highest- and lowest-frequency unstable modes; the corresponding corotating frame period P, inertial frame period[6] $P_{\rm i} \equiv 2\pi/(\sigma - m\,\Omega)$ and harmonic degree ratio $\tilde{\ell}/\ell$ are also tabulated. From the table, it is evident that a grand total of seven out of the 29 initially unstable PS modes are stabilized by the rotation. In the same way, the 94 non-PS modes that are initially unstable are augmented, upon the introduction of rotation, by the destabilization of a further 58; the largest gains, of 16 additional unstable modes, are accorded to the $(\ell, m) = (1, 1)$ group.

An important result clearly seen in Fig. 2 is that the stabilization or destabilization of modes, with varying rotation rate, does not suffice to maintain the boundaries of the instability at a constant frequency or period. For instance, the $(\ell, m) = (1, 1)$ modes mentioned above exhibit instability over the period range $\sim$1.05–1.95 d in the non-rotating case; but this range is narrowed and shifted to $\sim$0.65–1.05 d in the rapid-rotation limit. Thus, even though more modes are unstable in this limit, they occupy a narrower region of the pulsation spectrum; such behaviour is a direct consequence of the spectral compression discussed previously.

The processes selecting which modes are unstable are similar to those operative in a non-rotating star. As discussed by Dziembowski et al. (1993), one requirement for the κ mechanism to work efficiently is that the relative Lagrangian pressure perturbation $\delta p/p$ be large and slowly varying with radius within the excitation zone. This condition establishes the short-period limit of the instability at $|\tilde{n}| \sim 12$ (cf. Table 2); because the shape of radial eigenfunctions is insensitive to the strength of the Coriolis force (see, e.g., Ushomirsky & Bildsten 1998), this limit does not vary appreciably with rotation rate.

The corresponding long-period limit is determined not so much by the efficiency of the κ-mechanism driving, but more by the onset of significant thermal damping. This damping arises as a result of radiative diffusion between neighbouring fluid elements, operating primarily in a region of the envelope ($\log T \sim 5.9$) situated below the excitation zone. For the diffusion to be effective in stabilizing the pulsation requires a combination of long pulsation periods and high radial orders, the latter serving to steepen the temperature gradients driving the diffusion. The interplay between these two factors leads to a long-period instability limit that is quite sensitive to the rotation rate, as Fig. 2 attests.

4.2 Instability strips

The focus is now broadened, from the 53 Per-like model considered in the preceding section, to the complete set of stellar models introduced in Section 3. At three differing rotation rates, $\Omega/\Omega_{\rm c} = 0.0$, 0.25 and 0.5, BOOJUM is used to search for unstable $\ell = 1$ and $\ell = 2$ g modes; the results of these calculations are presented in Fig. 3, where the same HR diagram shown in Fig. 1 is overplotted by the instability strip associated with each (ℓ, m) combination at each rotation rate. These instability strips enclose all models that

[6] For retrograde modes, negative values of $P_{\rm i}$ (e.g. in the final row of Table 2) indicate the mode is prograde in the inertial frame.

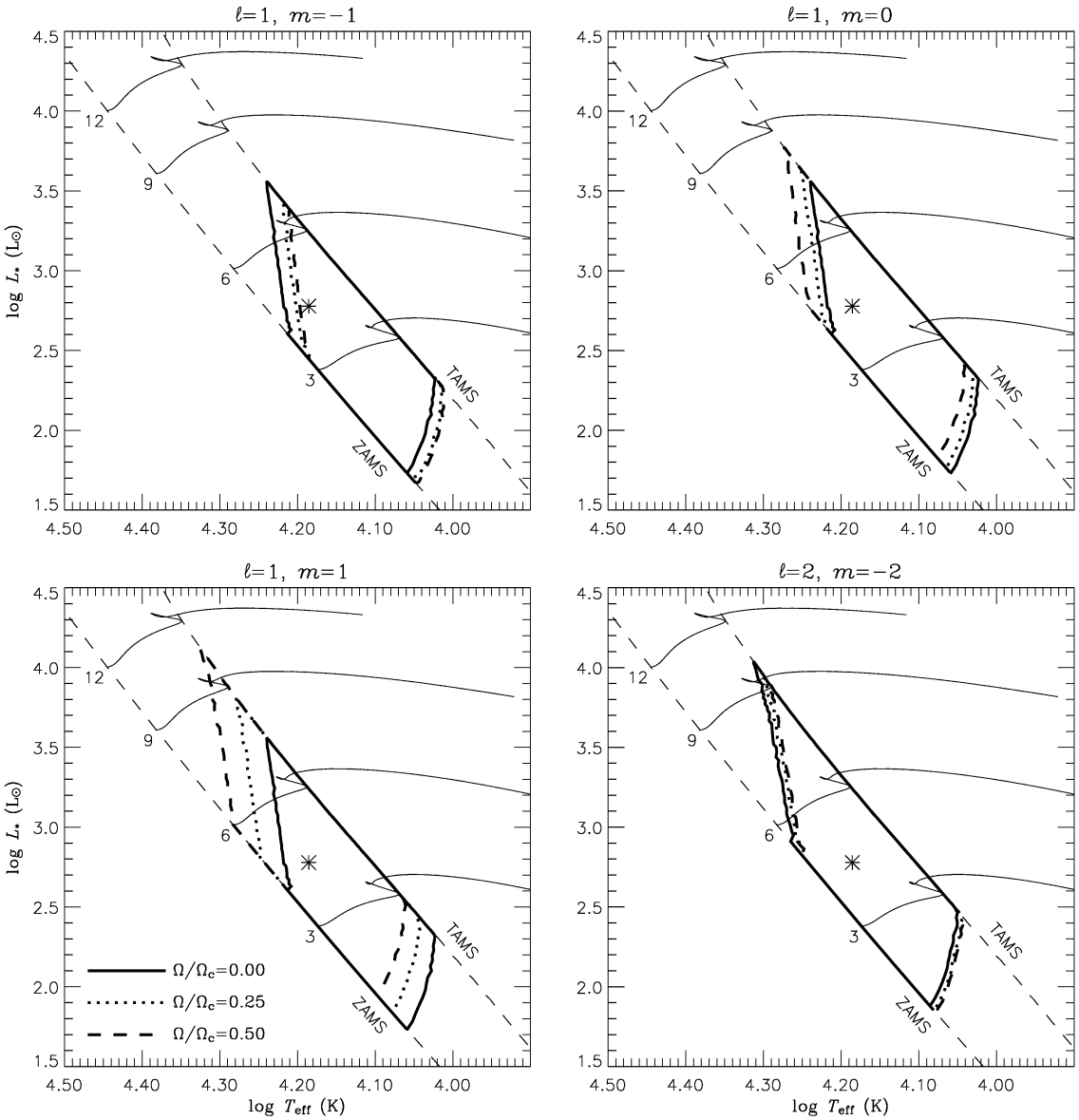

Figure 3. Instability strips in the Hertzsprung–Russell (HR) diagram, for $\ell = 1$ and $\ell = 2$ g modes of the stellar models introduced in Fig. 1. In each panel, corresponding to a particular combination (ℓ, m) of mode parameters, the extent of the κ-mechanism instability is indicated using thick lines, at the three differing rotation rates $\Omega/\Omega_c = 0.0$ (solid), 0.25 (dotted) and 0.5 (dashed) considered. The uneven boundaries of the instability strips, evident in some panels, are the result of the discrete spacing of the stellar models in the $T_{\rm eff}$–L_* plane.

are unstable ($\sigma_i < 0$) toward the excitation of one or more modes of the indicated type.

As with the preceding section, there is a clear division between the PS and the non-PS modes. The effect of rotation on the former is to shift their instability strips along the main sequence, toward lower temperatures and luminosities. The converse behaviour is exhibited by the latter, for which instability strips are shifted toward higher temperatures and luminosities. These shifts affect the blue edges of the instability to a greater degree than the corresponding red edges. For instance, the stellar models lying along the ZAMS are, in the absence of rotation, unstable toward $(\ell, m) = (1, 1)$ modes over the temperature range $4.06 \leqslant \log T_{\rm eff} \leqslant 4.21$. Upon the introduction of rotation, at the rate $\Omega/\Omega_c = 0.5$, this range shifts and broadens to $4.08 \leqslant \log T_{\rm eff} \leqslant 4.28$.

The behaviour of both classes of mode can be understood with reference to the prerequisites for excitation discussed by Dziembowski et al. (1993). In addition to the aforementioned restriction on the pressure eigenfunction (cf. Section 4.1), it is necessary that the thermal time-scale in the excitation zone be comparable to, or longer than, the pulsation period. This latter condition is the key to the behaviour seen in Fig. 3. The thermal time-scale

$$\tau_{\rm th}(r) = \frac{\int_r^{R_*} T c_p \, {\rm d}M_r}{L_*}, \tag{25}$$

evaluated at the radius where the opacity derivative κ_T is maximal, is a strong function of stellar effective temperature; it declines rapidly

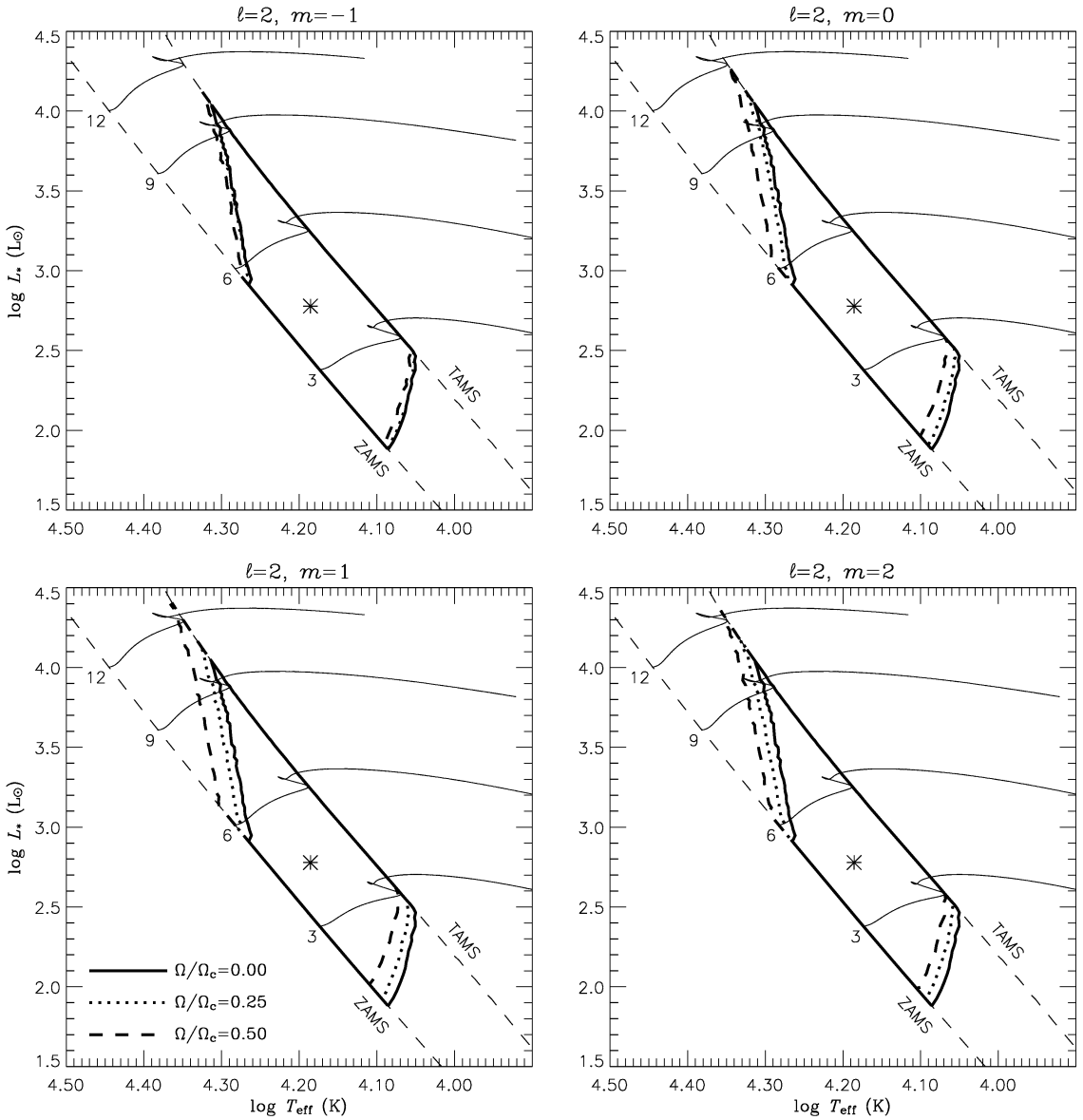

Figure 3 – *continued*

toward larger values of $T_{\rm eff}$, because the excitation zone[7] is situated ever closer to the surface. Consequently, for the non-PS modes, whose periods become shorter under the influence of the Coriolis force, the effect of rotation is to shift the instability toward stars having higher $T_{\rm eff}$, so that the $\tau_{\rm th}$–P matching condition can still be met. Conversely, for the PS modes, the marginal lengthening in periods as a result of rotation pushes the instability toward slightly lower $T_{\rm eff}$.

Fig. 4 illustrates these processes, by plotting instability regions in the $T_{\rm eff}$–P plane for stellar models situated along the ZAMS and TAMS boundaries. These regions, the complements of the instability strips shown in Fig. 3, indicate how the range of unstable-mode periods evolves with changing effective temperature; also shown in the figure, as separate curves for the ZAMS and the TAMS models, is the thermal time-scale within the excitation zone. For the non-PS modes, the period shortening caused by rotation is evidently responsible for the shift of the κ-mechanism instability toward higher effective temperatures, in order to maintain the loose correspondence between $\tau_{\rm th}$ and P. Likewise, for the PS modes, the period lengthening causes the instability to shift to lower effective temperatures, once again to keep $\tau_{\rm th}$ in step with P.

It is instructive to relate the foregoing analysis to previous studies (e.g. by Balona & Dziembowski 1999) of the effect that a varying harmonic degree ℓ has on the instability of SPB stars. It can be recognized that the pulsation equations (7)–(10) are, modulo a number of approximations, no different than those describing modes of harmonic degree $\tilde{\ell}$ *in a non-rotating star*. Accordingly, the influence of the Coriolis force on the period and stability of an individual mode can be followed simply by allowing $\tilde{\ell}$ to vary in some specified manner. For non-PS modes, this variation assumes the asymptotic form given in equation (24); clearly, any increase in ν, corresponding to

[7] Typically occurring at a temperature $\log T \approx 5.3$.

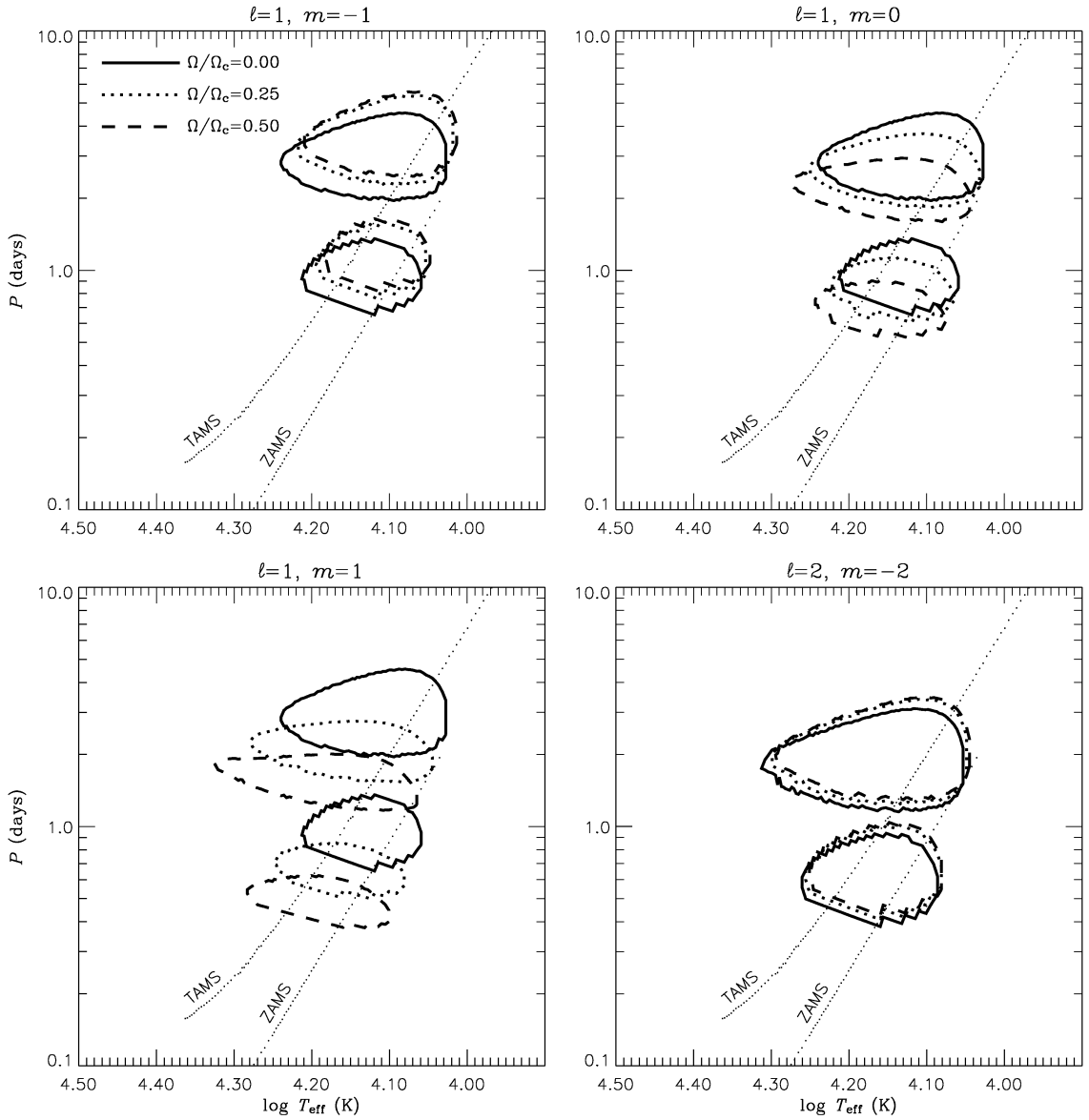

Figure 4. Instability regions in the $T_{\rm eff}$–P plane, for $\ell = 1$ and $\ell = 2$ g modes of stellar models lying along the zero-age main sequence (ZAMS) and terminal-age main sequence (TAMS) boundaries (cf. Fig. 1). In each panel, corresponding to a particular combination (ℓ, m) of mode parameters, the extent of the κ-mechanism instability is indicated using thick lines, at the three differing rotation rates $\Omega/\Omega_{\rm c} = 0.0$ (solid), 0.25 (dotted) and 0.5 (dashed) considered. The points, comprising separate curves for the ZAMS and the TAMS models, indicate the thermal time-scale $\tau_{\rm th}$ within the excitation zone.

more-rapid rotation, leads to a proportional increase in $\tilde{\ell}$. However, as the instability strips presented by Balona & Dziembowski (1999, their fig. 5) reveal, the result of raising the harmonic degree is to shift the g-mode instability toward higher luminosities and effective temperatures: exactly the behaviour manifested in the blueward displacement, at higher rotation rates, of the instability strips plotted in Fig. 3. A similar line of reasoning can be applied to the PS modes.

Although these parallels to the non-rotating case are instructive, an important caveat should be made regarding their use. Reiterating the fact that the spin parameter ν is itself a function of the pulsation frequency σ, it is clear that the effective harmonic degree $\tilde{\ell}$ assumes different values even among modes having the same true harmonic degree ℓ and azimuthal order m. This result, already discussed in Section 4.1 under the guise of spectral compression, is why the Coriolis force tends not only to shift the κ-mechanism instability strips for SPB stars, but also acts to broaden them.

5 DISCUSSION AND SUMMARY

In the preceding sections, an approximate method for treatment of the Coriolis force (Section 2.1) is used to devise equations governing non-adiabatic, non-radial pulsation of rotating stars (Sections 2.2). These equations are solved (Section 2.3) for a range of mid-B-type stellar models (Section 3); the general finding (Section 4) is that the Coriolis force shifts the instability strip associated with κ-mechanism excitation of g modes toward higher luminosities and effective temperatures for non-PS modes, and toward lower luminosities and effective temperatures for PS modes.

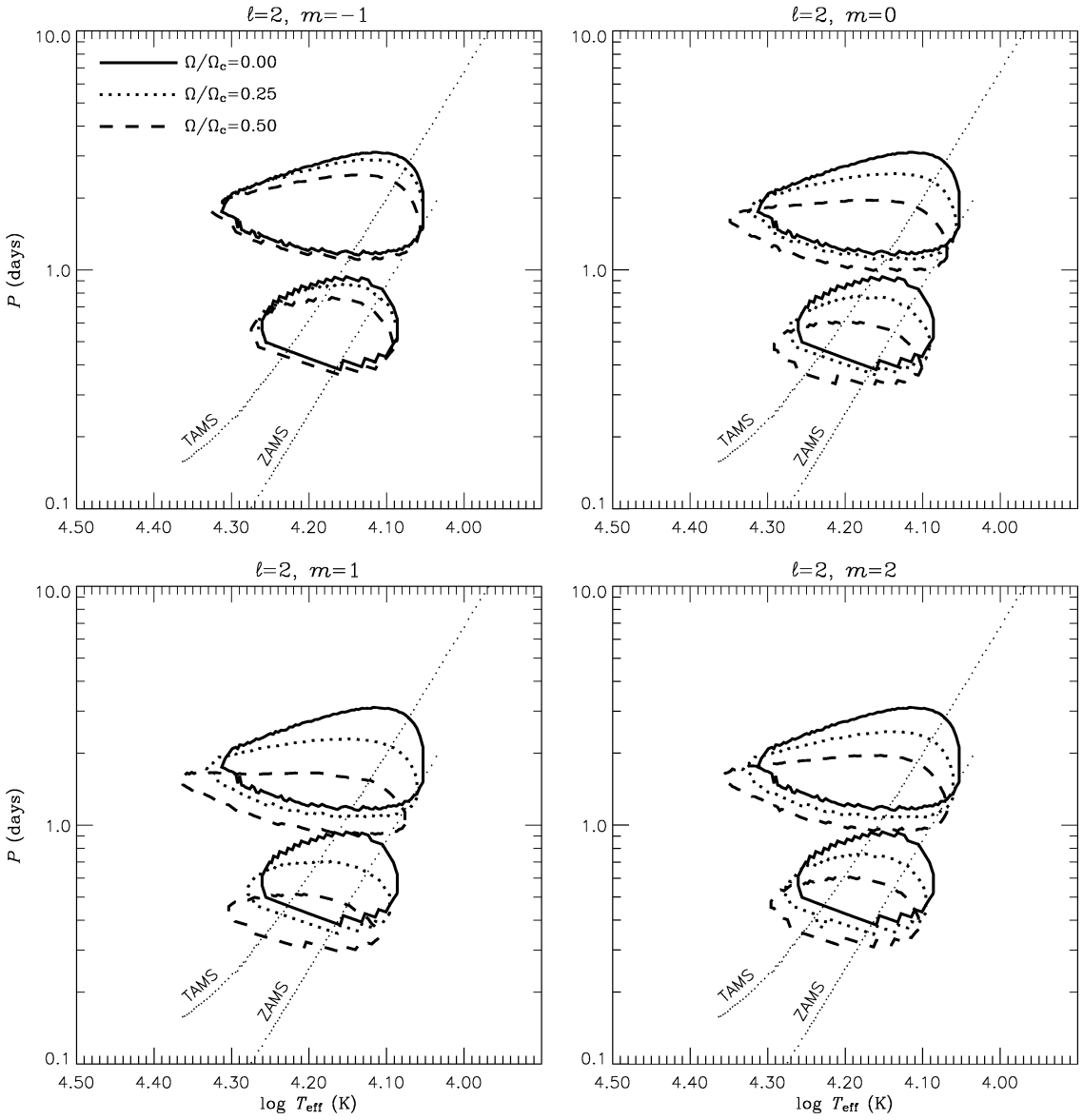

Figure 4 – *continued*

An immediate corollary of this result is that the Coriolis force is unable to stabilize *all* B-type stars against g mode pulsation; rather, it can only alter which particular stars, at a given rotation rate, are unstable. Similar conclusions were reached by Ushomirsky & Bildsten (1998) in their quasi-adiabatic analysis, and by Lee (2001) in his complete treatment of the Coriolis force. However, as discussed in Section 1, observations of SPB stars reveal an apparent paucity of objects rotating at significant rates. How might this discrepancy between theory and observations be resolved?

One possibility is that the centrifugal force, neglected in the present treatment and by Lee (2001), can act to stabilize modes. Certainly, not taking this force into account will introduce a certain level of error in the results, especially at the upper limit $\Omega/\Omega = 0.5$ adopted herein, which comes very close to violating the assumption (cf. Section 2.1) that $\Omega^2 \ll \Omega_c^2$. However, Lee & Baraffe (1995) and Lee (1998) have demonstrated that the centrifugal force has little effect on the stability of the g modes characteristic to SPB stars. Perhaps a more plausible scenario is that resonant coupling, between modes of differing harmonic degree (see, e.g., Chandrasekhar & Lebovitz 1962), may act to suppress the κ-mechanism instability. These couplings, which are neglected in the present analysis because of the adoption of the traditional approximation, were shown by Lee (2001) to inhibit the excitation of selected modes that would otherwise be unstable in rotating SPB stars.

Nevertheless, it is highly unlikely that resonant coupling could suppress the instability of all modes. With this in mind, it appears increasingly probable that, as the theoretical analysis indicates, g modes *are* excited in rotating SPB stars; but that the equatorial-confinement effects demonstrated by Townsend (2003b) render them very difficult to detect observationally. In support of this interpretation for the observational scarcity of rotating SPB stars, two of the open clusters originally thought to be devoid of SPB stars,

NGC 4755 (Balona & Koen 1994) and NGC 6231 (Balona & Laney 1995), have, upon closer scrutiny, been found to contain a number of candidate-SPB objects (see Stankov et al. 2002; Arentoft et al. 2001).

In addition to their direct applicability to SPB stars, the results presented herein are highly relevant to the understanding of the Be phenomenon. The multiperiodic spectroscopic and photometric variations exhibited by many Be stars (e.g. μ Cen, Rivinius et al. 1998; ω CMa, Štefl et al. 2003) are usually interpreted as arising from non-radial g modes (see Rivinius, Baade & Štefl 2003, and references therein). It is not unreasonable to suppose the excitation of these modes to be the result of the same κ mechanism operative in the SPB stars. However, a historical problem with this stance has been that many variable Be stars have early spectral types B0–B3, falling bluewards of the high-temperature limit of the SPB instability strip for low-degree pulsation (Balona & Dziembowski 1999). Furthermore, periodic variations are not seen in Be stars with types later than B5 (e.g. Baade 1989a,b, and references therein), even though the SPB instability strip extends all the way down to types B8 or B9.

Both of these difficulties are resolved by allowing for the influence of the Coriolis force, which, as the present analysis demonstrates, has the effect of shifting κ-mechanism instability toward earlier spectral types. Of course, this rationalization can only work if the modes seen in Be stars are not PS; however, in light of the analysis presented by Rivinius et al. (2003), who found at least 16 of the 27 Be stars in their sample to pulsate in retrograde $(\ell, m) = (2, 2)$ modes, this latter restriction does not appear to be problematic.

ACKNOWLEDGMENTS

I thank Stan Owocki and Myron Smith for their helpful suggestions, and the referee Prof. W. Dziembowski for his insightful remarks. This research has been partially supported by US NSF grant AST-0097983, and by the UK Particle Physics and Astronomy Research Council. Computations were undertaken on the Parameter Search Engine at the HiPerSPACE Computing Centre, UCL, which is funded by PPARC.

REFERENCES

Anderson E. et al., 1999, LAPACK Users' Guide, 3rd edn. Society for Industrial and Applied Mathematics, Philadelphia
Arentoft T., Sterken C., Knudsen M. R., Freyhammer L. M., Duerbeck H. W., Pompei E., Delahodde C. E., Clasen J. W., 2001, A&A, 380, 599
Baade D., 1989a, A&AS, 79, 423
Baade D., 1989b, A&A, 222, 200
Balona L. A., 1994, MNRAS, 267, 1060
Balona L. A., 2000, in Szabados L., Kurtz D. W., eds, ASP Conf. Ser. Vol. 203; Proc. IAU Colloq. 176, The Impact of Large-Scale Surveys on Pulsating Star Research. Astron. Soc. Pac., San Francisco, p. 401
Balona L. A., Dziembowski W. A., 1999, MNRAS, 309, 221
Balona L. A., Koen C., 1994, MNRAS, 267, 1071
Balona L. A., Laney C. D., 1995, MNRAS, 276, 627
Balona L. A., Laney C. D., 1996, MNRAS, 281, 1341
Bildsten L., Ushomirsky G., Cutler C., 1996, ApJ, 460, 827
Carroll B. W., Hansen C. J., 1982, ApJ, 263, 352
Castor J. I., 1971, ApJ, 166, 109
Chandrasekhar S., Lebovitz N. R., 1962, ApJ, 136, 1105
Christensen-Dalsgaard J., Mullan D. J., 1994, MNRAS, 270, 921
Cowling T. G., 1941, MNRAS, 101, 367
De Ridder J., Gordon K. D., Mulliss C. L., Aerts C., 1999, A&A, 341, 574
Dziembowski W. A., 1971, Acta Astron., 21, 289
Dziembowski W. A., Pamyatnykh A. A., 1993, MNRAS, 262, 204
Dziembowski W. A., Moskalik P., Pamyatnykh A. A., 1993, MNRAS, 265, 588
Eckart C., 1960, Hydrodynamics of Oceans and Atmospheres. Pergamon Press, Oxford
Gill A. E., 1982, Atmosphere–Ocean Dynamics. Academic Press, London
Grevesse N., Noels A., 1993, in Pratzos N., Vangioni-Flam E., Cassé M., eds, Origin and Evolution of the Elements. Cambridge Univ. Press, Cambridge, p. 15
Iglesias C. A., Rogers F. J., 1996, ApJ, 464, 943
Kahan W., 1966, Technical Report CS41, Accurate Eigenvalues of a Symmetric Tridiagonal Matrix. Computer Science Dept., Stanford University, Stanford
Ledoux P., 1951, ApJ, 114, 373
Lee U., 1998, ApJ, 497, 912
Lee U., 2001, ApJ, 557, 311
Lee U., Baraffe I., 1995, A&A, 301, 419
Lee U., Saio H., 1987a, MNRAS, 224, 513
Lee U., Saio H., 1987b, MNRAS, 225, 643
Lee U., Saio H., 1990, ApJ, 349, 570
Lee U., Saio H., 1997, ApJ, 491, 839
Lighthill J., 1978, Waves in Fluids. Cambridge Univ. Press, Cambridge
Mathias P., Aerts C., Briquet M., De Cat P., Cuypers J., Van Winckel H., Flanders. Le Contel J. M., 2001, A&A, 379, 905
Muller D. E., 1956, Math. Tab. Aids Comput., 10, 208
Osaki J., 1975, PASJ, 27, 237
Osaki Y., Hansen C. J., 1973, ApJ, 185, 277
Pamyatnykh A. A., 1999, Acta Astron., 49, 119
Pesnell W. D., 1990, ApJ, 363, 227
Press W. H., Teukolsky S. A., Vetterling W. T., Flannery B. P., 1992, Numerical Recipes in Fortran, 2nd edn. Cambridge Univ. Press, Cambridge
Rivinius T., Baade D., Štefl S., Stahl O., Wolf B., Kaufer A., 1998, A&A, 336, 177
Rivinius T., Baade D., Štefl S., 2003, A&A, 411, 229
Rogers F. J., Swenson F. J., Iglesias C. A., 1996, ApJ, 456, 902
Saio H., Cox J. P., 1980, ApJ, 236, 549
Savonije G. J., Papaloizou J. C. B., Alberts F., 1995, MNRAS, 277, 471
Scuflaire R., 1974, A&A, 36, 107
Smith M. A., 1977, ApJ, 215, 574
Stankov A., Handler G., Hempel M., Mittermayer P., 2002, MNRAS, 336, 189
Štefl S., Baade D., Rivinius T., Stahl O., Budovičová A., Kaufer A., Maintz M., 2003, A&A, 411, 167
Sugimoto D., 1970, ApJ, 159, 619
Takata M., Löffler W., 2004, PASJ, 56, 645
Townsend R. H. D., 2000, MNRAS, 319, 289
Townsend R. H. D., 2003a, MNRAS, 340, 1020
Townsend R. H. D., 2003b, MNRAS, 343, 125
Townsend R. H. D., 2004, in Maeder A., Eenens P., eds, Proc. IAU Symp. 215, Stellar Rotation. Astron. Soc. Pac., San Francisco, p. 404
Traub J. F., 1964, Iterative Methods for the Solution of Equations. Prentice-Hall, Englewood Cliffs
Unno W., Osaki Y., Ando H., Saio H., Shibahashi H., 1989, Nonradial Oscillations of Stars, 2nd edn. University of Tokyo Press, Tokyo
Ushomirsky G., Bildsten L., 1998, ApJ, 497, L101
Waelkens C., 1991, A&A, 246, 453
Waelkens C., Rufener F., 1985, A&A, 152, 6

This paper has been typeset from a TEX/LATEX file prepared by the author.